Hydrogen recovery from steam methane reforming using the ITQ-12 zeolite

Separation and Purification Technology 350 (2024) 127895

Contents lists available at ScienceDirect

Separation and Purification Technology

journal homepage: www.elsevier.com/locate/seppur

Hydrogen recovery from steam methane reforming using the ITQ-12 zeolite

Jeroen van Heijst [a], Ana Martin-Calvo [b,*], Sofia Calero [a,*]

[a] Department of Applied Physics, Eindhoven University of Technology, Eindhoven, The Netherlands
[b] Center for Nanoscience and Sustainable Technologies (CNATS), Universidad Pablo de Olavide, Seville, Spain

ARTICLE INFO

Keywords:
Monte Carlo
Molecular simulations
Purification
Breakthrough
Hydrogen
Zeolites

ABSTRACT

The aim of this work is to investigate the potential use of the ITQ-12 zeolite in a PSA process to obtain purified hydrogen from the SMR product stream using molecular simulation. Since the main components of the product stream are hydrogen and carbon dioxide, we put the focus on the separation of these two gases. The separation of hydrogen from the other components (methane, carbon monoxide and nitrogen) will be briefly touched upon as well. From inspection of the adsorption isotherms of carbon dioxide and hydrogen in ITQ-12 we found that the former gas dominates at industrially relevant conditions (311 K and 16 $\cdot 10^5$ Pa). Breakthrough curves reveal that the ITQ-12 zeolite is likely to perform well in a PSA process for the separation of hydrogen from carbon dioxide. We found that in general higher column lengths and lower gas feed velocities are favorable for a good separation while higher gas feed velocities are favorable for the cleansing of carbon dioxide from the column. For the full mixture it is necessary to employ longer column lengths in order to separate hydrogen from the other components. This is because nitrogen and carbon monoxide exhibit retention times similar to hydrogen, though the latter still travels through the column the fastest. Alternatively the use of ITQ-12 could be combined with other separation techniques, where ITQ-12 is used to mainly remove CO_2 and CH_4 from the SMR product stream. These findings suggest that SMR could become an economically viable way to produce hydrogen by using ITQ-12 in the separation process.

1. Introduction

Hydrogen is a promising contender for becoming the fuel of the future. This is largely due to the fact that it can be more conveniently stored than electricity and does not produce any harmful emissions when used as a fuel [1]. These qualities make hydrogen an excellent energy carrier that can potentially be used for example in combination with solar energy to power households in the future. A popular industrial process for the production of hydrogen gas from natural gas is steam methane reforming (SMR) [2–4]. While there are many competing technologies under development, SMR is potentially useful in the early stages of the hydrogen economy, when the demand for hydrogen is still comparatively low and supply can be based on small scale and decentralized SMR or electrolysis [2]. The advantage of such decentralized hydrogen production is that existing natural gas pipelines can be used to transport natural gas to the SMR plants. Therefore there is no immediate need for extensive hydrogen infrastructure.

Like any modern chemical process, steam methane reforming consists of multiple steps. In the first step, natural gas is purified to methane [5]. Natural gas is a mixture of consisting mostly of methane, but also of other alkanes as well as gases such as carbon dioxide, nitrogen, helium, hydrogen sulfide and some other sulfide compounds. The most important step of the process is the reforming reaction of methane with water. This produces hydrogen along with carbon monoxide and carbon dioxide [5]. See Eqs. (1) and (2).

$$CH_4 + 2H_2O \rightarrow 4H_2 + CO_2 \quad (1)$$

$$CH_4 + H_2O \rightarrow 3H_2 + CO \quad (2)$$

This mixture then passes through the water–gas shift reactor. This reactor uses water to convert most of the carbon monoxide into carbon dioxide and hydrogen [5]. See Eq. (3).

$$CO + H_2O \leftrightarrow CO_2 + H_2 \quad (3)$$

This is an equilibrium reaction for which the equilibrium concentration of CO_2 is higher at lower temperatures. Unfortunately the reaction rate is too low at low temperatures. To remedy this issue, the water–gas shift reaction is usually split up into two parts: the high temperature shift reactor and the low temperature shift reactor. First the higher temperature is used to speed up the reaction rate, and then the lower temperature is used to increase the amount of CO_2 and H_2 that is produced [6]. Finally the resulting gas mixture consisting mostly of

* Corresponding authors.
E-mail addresses: amarcal@upo.es (A. Martin-Calvo), s.calero@tue.nl (S. Calero).

https://doi.org/10.1016/j.seppur.2024.127895
Received 7 March 2024; Received in revised form 6 May 2024; Accepted 7 May 2024
Available online 10 May 2024

carbon dioxide and hydrogen (but also containing traces of methane, nitrogen and carbon monoxide [7]) is purified.

There are still some hurdles to overcome in order to make this process more economically viable. For example production should be made more user friendly, the cost should be decreased and it is important to improve the recovery of hydrogen from the product stream. This work will focus on the latter. In other words the question to be answered is how to improve hydrogen capture from an SMR product stream. A possible way to do this is by using a porous material such as a zeolite. Zeolites are a porous class of materials often used for the separation of fluids through adsorption. Apart from zeolites there are some other porous classes of chemical substances that are commonly used for adsorption purposes. These include activated carbons (AC's) and metal organic frameworks (MOF's). The reason to use a zeolite is that it is more thermochemically stable and often available at relatively low costs compared to for example MOF's [8,9]. The main idea when applying a zeolite for the separation of two fluids is that one of the fluids will be adsorbed into the zeolite at a higher rate than the other. In the case of a binary mixture the two fluids can be easily separated using a process such as pressure swing adsorption (PSA) [5,10–13].

To investigate the feasibility of using a zeolite for purification, it is important to take into account the conditions of the mixture as it exits the low temperature shift reactor (at which point the purification takes place). While these conditions vary per setup, the results in this work will be based on the conditions reported by J. C. Molburg and R. D. Doctor [6]. This will be discussed in more detail in the Methodology section.

This work focuses specifically on the ITQ-12 zeolite. ITQ-12, also referred to as ITW, is a pure silica zeolite, meaning that it consists purely of silicon and oxygen atoms, with no aluminium substitutions. Visualizations of the unit cell of the structure are included in Figure S1 of the Electronic Supporting Information (ESI). The structure consists of cavities and channels made out of 8-rings, meaning that ITQ-12 is a small-pore-zeolite [8]. The structure admits two types of channels [14] (see also Figure S2 in the ESI). One channel is along the (100) direction and is relatively narrow: (2.4 × 5.3 Å). The other is among the (001) direction and is more circular (3.8 × 4.1 Å) and connects bigger cavities. Since ITQ-12 is a small pore zeolite, it is likely to be suitable for separating different kinds of small molecules from one another. It has already been shown that ITQ-12 can be used to effectively separate propane from propene [15,16] and carbon dioxide from methane [17]. This begs the question whether the zeolite is also a useful 'sieve' for separating hydrogen from carbon dioxide and the other components in the SMR product stream. To answer this question use will be made of adsorption isotherms and breakthrough curves computed using molecular simulation in RASPA and RUPTURA [18,19].

Summarizing, in this work simulation techniques are used for the first time to study the recovery of hydrogen from the SMR product stream using the ITQ-12 zeolite, by means of adsorption isotherms and specially by means of breakthrough curves. An optimization of the breakthrough "setup" in terms of column length and gas feed velocity is investigated for an efficient separation. The effect of minor components of the real product stream composition is analyzed by comparison with the results obtained from the simplified SMR product stream.

The methods, models and forcefields used for simulations, as well as the mixture under study and the characterization of the material are described in the Methodology section. The results section includes a discussion of the main findings from the force-field validation, adsorption isotherms and breakthrough curves for a simplified version of the SMR product stream and for the stream with all its components. Finally, the main conclusions of the work are drawn.

2. Methodology

The results in this work are based on the conditions reported by J. C. Molburg and R. D. Doctor [6]. Therefore a temperature of 311 K and a pressure of 16 bar ($16 \cdot 10^5$ Pa) will be used. Additionally, the simulations in this work will be based on the mixture composition included in Table 1. The initial results of this work will be limited to investigating only the main components hydrogen and carbon dioxide. Hence use will be made of a mixture containing 0.2 molar fraction CO_2 and 0.8 molar fraction H_2 (keeping the same relative concentration between CO_2 and H_2 as in Table 1). Later the mixture will be studied in more detail. For this the choice was made to leave water out of the consideration since it can be removed via other methods. This means the concentrations mentioned in the rightmost column of Table 1 are used.

Table 1
Composition of product stream to be purified according to the work of J. C. Molburg and R. D. Doctor [6], as well as concentrations used in this work, disregarding water.

Component	Molar fraction [–]	Without water [–]
CO_2	0.13281	0.18505
CO	$7.43587 \cdot 10^{-4}$	$1.03615 \cdot 10^{-4}$
H_2O	0.28235	0
H_2	0.53182	0.74106
CH_4	0.04939	0.06882
N_2	0.00288	0.00401

In this work the RASPA software is used to simulate the interaction of various zeolites and adsorbates [18]. More specifically, Grand Canonical Monte Carlo (GCMC) simulations will be used to compute adsorption isotherms for single components as well as mixtures. The use of a Grand Canonical ensemble means that the chemical potential is fixed, as well as the temperature and the volume. The chemical potential is related to fugacity and pressure through the Peng–Robinson equations of state [18]. Monte Carlo simulations make use of a set of moves that are applied to fluid elements at random [20]. The allowed moves vary per setting and include translation, rotation and insertion, as well as identity change in case of mixtures. When such a random move is tried it can be either accepted or rejected. In the latter case nothing happens. Whether a move is accepted or rejected is based on energy criteria. The random moves make sure that the system will ultimately end up in an equilibrium situation. To make sure that this equilibrium is reached in the simulation it is important to make use of an adequate number of cycles. In the case of Monte Carlo simulations, a cycle consists of $\max(N, 20)$ attempted moves, where N is the amount of molecules. 80000 initialization cycles and 800000 regular cycles were used for all adsorption isotherm computations. The output of this type of simulation in RASPA is the total amount of molecules located inside the pores of the structure, which is referred to as the absolute adsorption. However, experimental measurements exclude the molecules that are in the pores without gas–solid interaction, giving rise to the excess adsorption. For this reason, to compare simulated and experimental data it is necessary to convert absolute (n_{abs}) into excess (n_{exc}) adsorption using Eq. (4).

$$n_{\text{exc}} = n_{\text{abs}} - V_g \rho_g \tag{4}$$

Here V_g is the pore volume of the adsorbent, and ρ_g is the molar density of the bulk gas phase [21]. The available pore volume can be obtained experimentally or by simulation measuring He/N_2 adsorption as explained the discussion of the framework models used.

To accurately model the process of adsorption, three components have to be considered. These components are the framework, the adsorbates and the forcefield (i.e. the interactions between the different components).

To simulate the framework it is assumed that the silicon and oxygen atoms are simply fixed. This modeling assumption has been shown to have little effect on the accuracy of the computed adsorption isotherms [22]. Three separate models for the framework were considered before the validation of the modeling methods. These models were named ITQ-12 [14], ITQ-12bis [16] and ITW. The ITQ-12bis

Table 2
Comparison of framework models and experimental data by E. Pérez-Botella *et al.* [17].

Framework model	Helium void fraction [–]	Specific surface area [m^2/g]	Available pore volume [cm^3/g]
ITQ-12	0.1732 ± 0.0002	352.3 ± 0.4	0.097
ITQ-12bis	0.15964 ± 0.00010	334.7 ± 0.2	0.088
ITW	0.1814 ± 0.0001	388.7 ± 2	0.10
Experimental	–	356	0.18

and ITW structures can be obtained from the IZA-SC Database of Zeolite Structures [23]. The former two structures correspond to actual synthesized instances of the zeolite and their reported topologies, while the latter constitutes a theoretical structure. Table 2 contains the values of the helium void fraction, specific surface area and available pore volume for all three framework models as well as the experimental values reported by E. Pérez-Botella et al. [17]. This article was used for comparison between adsorption isotherms computed using the three models and experimental data for both CO_2 and CH_4. Additionally, the pore size distribution has been computed for all three framework models. The result of this is included in Figure S3 of the ESI. The helium void fraction is computed using the Widom particle insertion method [24] (using 500000 MC cycles). The specific surface area is computed geometrically by 'rolling' a nitrogen probe along the surface of the zeolite [21,25,26] (using 10000 MC cycles). The available pore volume is computed using the framework density d and the helium void fraction (HVF) according to Eq. (5).

$$\text{Available pore volume} = \frac{\text{HVF} \cdot 100}{d} \tag{5}$$

Here the density of the ITQ-12 zeolite is 1792 kg/m^3 (according to the adsorption isotherm simulations performed in RASPA). The pore size distribution is computed using the method of Gelb and Gubbins [26,27] and an MC volume integration method (using 10000 MC cycles). In Table 2 it can be noticed that in particular ITQ-12 and ITQ-12bis exhibit significantly smaller available pore volumes compared to the experimental data. Additionally their specific surface area is also somewhat lower compared to experimental data. ITW on the other hand has a significantly higher available pore volume which is in better agreement with the experimental data. Additionally its specific surface area is significantly higher and actually exceeds the specific surface area that was found experimentally. Helium void fractions do not differ that radically between the three theoretical structures. Since this work is aimed at industrial practice it was chosen to continue with either ITQ-12 or ITQ-12bis as these are real-life instances of the material. Ultimately the agreement with experimental data was better for ITQ-12 which led to the choice to continue with the ITQ-12 model for later simulations.

For the adsorbates, previously established models were taken from literature. Nitrogen [28], carbon monoxide [29] and carbon dioxide [30] are described using full atom models with Lennard-Jones parameters and point changes in all atoms. Dummy atoms are used to reproduce the dipole and quadrupole moments of CO and N_2 respectively. For methane [31] and hydrogen [9] united atom models are used. The model for hydrogen includes quantum corrections, achieved through use of the Feynman–Hibbs effective interaction potential. All these models have been previously validated to reproduce experimental properties of the molecules as vapor pressure, vapor liquid equilibria or liquid density and to be transferable to different zeolites [9,28–31]. All charges and Lennard-Jones parameters are collected in Table 3.

To model the forcefield, its components are separated into two categories, bonding (bonding, bending, torsion) and anti-bonding (electrostatic, Van der Waals) forces [32]. The bonding forces are specified per adsorbate. For hydrogen and methane there is no need to specify these since they are modeled using a united atom model. For carbon dioxide, nitrogen and carbon monoxide the atomic bonds are modeled as rigid and therefore there is again no need to specify the bonding energies to compute the relative positions of atoms in the molecule. The anti-bonding forces consist of Van der Waals and electrostatic forces. Van der Waals forces are generally computed using Lennard-Jones parameters. The general mixing rule used for Lennard-Jones is Lorentz–Berthelot [33]. For hydrogen Feynman–Hibbs–Lennard-Jones parameters are used instead of Lennard-Jones in order to accurately model the non-negligible quantum effects that occur at low temperatures [9]. For the silicon atoms the Van der Waals force is neglected since this is largely screened by the surrounding oxygen atoms [22]. Electrostatic forces are based on simple coulomb potentials. To compute the electrostatic forces, use is made of Ewald summation [34]. For both types of anti-bonding forces, a cutoff distance needs to be specified to reduce computational complexity. Potentials are truncated at this cutoff distance and then shifted downward so that they are equal to zero at the cutoff. The cutoff distance is chosen to be at 12 Å. Table 3 contains the parameter values used for calculating the interactions of components with themselves. For the silicon and oxygen atoms in the zeolite this is not needed since the framework is modeled as rigid. Table 4 contains the parameter values for calculating the interactions between adsorbates and zeolite atoms (these calculations also use the charges from Table 3). Parameter values for adsorbate interactions with themselves and zeolite atoms were taken from literature.

While the results of this work concern the ITQ-12 zeolite, the MFI zeolite is also used in simulations in order to validate the methods used. Since MFI is also a pure silica zeolite, no additional interactions have to be specified in the forcefield. The structure used for the MFI zeolite was taken from the work of H. van Koningsveld et al. [35]. Since the size of the unit cells of these zeolites varies, how many unit cells are used for the simulations needs to be determined with care. For the MFI zeolite, 2 × 2 × 2 unit cells were used to perform the simulations.

Table 3
Self-interactions defined for the zeolite and adsorbate atoms/molecules. General mixing rule used for Lennard-Jones is Lorentz–Berthelot. Nitrogen [28], carbon monoxide [29] and carbon dioxide [30] are described using full atom models with Lennard-Jones parameters and point changes in all atoms. For methane [31] and hydrogen [9] united atom models are used. Quantum corrections for the hydrogen model are achieved through use of the Feynman–Hibbs effective interaction potential.

Zeolite atom	Interaction type				Charge [e]
Si	None				0.78598
O	None				−0.39299
Adsorbate atom/molecule	**Interaction type**	**ϵ/k_B [K]**	**σ [Å]**	**Reduced mass [u]**	**Charge [e]**
H_2	Feynman–Hibbs–Lennard-Jones	36.733	2.958	1.0	0.0
CH_4	Lennard-Jones	158.5	3.72		0.0
O (in CO_2)	Lennard-Jones	85.671	3.017		−0.3256
C (in CO_2)	Lennard-Jones	29.93	2.742		0.6512
O (in CO)	Lennard-Jones	98.014	2.979		−0.2744
C (in CO)	Lennard-Jones	16.141	3.363		−0.2424
N (in N_2)	Lennard-Jones	38.298	3.306		−0.4048

Table 4
Interactions between adsorbates and framework atoms defined in the forcefield. Nitrogen [28], carbon monoxide [29] and carbon dioxide [30] are described using full atom models with Lennard-Jones parameters and point changes in all atoms. For methane [31] and hydrogen [9] united atom models are used. Quantum corrections for the hydrogen model are achieved through use of the Feynman–Hibbs effective interaction potential.

Adsorbate atom/molecule	Zeolite atom	Interaction type	ϵ/k_B [K]	σ [Å]	Reduced mass [u]
H_2	O	Feynman–Hibbs–Lennard-Jones	66.055	2.890	1.79
H_2	Si	Feynman–Hibbs–Lennard-Jones	28.256	1.854	1.88
CH_4	O	Lennard-Jones	115.00	3.47	
O (in CO_2)	O	Lennard-Jones	78.98	3.237	
C (in CO_2)	O	Lennard-Jones	37.595	3.511	
O (in CO)	O	Lennard-Jones	98.839	3.057	
C (in CO)	O	Lennard-Jones	40.109	3.379	
N (in N_2)	O	Lennard-Jones	60.58	3.261	

For the ITQ-12 zeolite 3 × 3 × 3 unit cells were used to perform the simulations.

Apart from adsorption isotherms, breakthrough curves are also of interest. To allow for the computation of breakthrough curves, it is necessary to use a mathematical model to fit the pure component adsorption isotherms. Adsorption isotherms are fitted using RUPTURA. This process consists both of identifying which theoretical model fits the simulation data the best and determining the parameters that allow for a good fit of the model. RUPTURA offers a variety of fitting methods. Examples of these include the Sips [36], Toth [37–39], Freundlich [40], Langmuir [41] and Langmuir–Freundlich [42] models. In this work use will be made of Langmuir and Langmuir–Freundlich models. The Langmuir method makes use of a single isotherm site. For the Langmuir–Freundlich models the use of one, two or three isotherm sites is considered. This means that, in total, four different candidates are considered for the fitting. Out of these the best performing model will be used. The found values for the fitting parameters play an important role in the simulation of breakthrough curves and mixture adsorption isotherms using RUPTURA. For hydrogen, nitrogen, methane and carbon monoxide the best performing model was found to be the Langmuir–Freundlich model with two isotherm sites. For carbon dioxide the best performing model was found to be the Langmuir–Freundlich model with three isotherm sites. The equation used for the fitting of an n-site Langmuir–Freundlich model is given by Eq. (6).

$$q(p) = \sum_{i=1}^{n} q_i^{\text{sat}} \frac{b_i p^{v_i}}{1 + b_i p^{v_i}} \tag{6}$$

Here q denotes the absolute loading in mol per kg zeolite at pressure p (in Pa), q_i^{sat} denotes the saturation capacity in mol per kg zeolite for the ith isotherm site, b_i denotes the dimensionless coefficient of adsorption for the ith isotherm site, representing the affinity of the molecule to be adsorbed and v_i denotes the dimensionless heterogeneity factor for the ith isotherm site, which accounts for the heterogeneity in adsorption sites. Further details can be found in the work of S. Sharma et al. [19]

The fitting parameters from the best fit will be used to compute predicted mixture adsorption isotherms. This will be done for the mixture containing only CO_2 and H_2 as well as the more detailed mixture which excludes only water, see Table 1. These predicted mixture adsorption isotherms will be computed using Ideal Adsorption Solution Theory (IAST) in RUPTURA. To allow for a meaningful comparison the isotherms will be computed at a temperature of 311 K. The mixture prediction comparison is used to verify whether mixture prediction using IAST can be used for breakthrough curve simulations. RUPTURA also offers several alternatives to IAST (SIAST, EI and SEI) that could be used in case of bad agreement.

For the computation of breakthrough curves, use is made of the RUPTURA software (see section 4.7 in the work of S. Sharma et al. [19] for a detailed description of the methodology). Once again IAST is used for these computations. Besides the fitting parameters there are still a lot of other parameters that need to be specified for this computation. First of all the breakthrough curve is computed for both the CO_2/H_2 mixture (i.e. 0.2 molar fraction CO_2, 0.8 molar fraction H_2) and the more detailed mixture (see Table 1). These breakthrough curves are computed at the conditions at which the SMR product stream leaves the reaction, meaning 311 K and 16 $\cdot 10^5$ Pa. Additionally, use is made of helium, which serves as a carrier gas. Therefore, for both simulations use is made of a gas stream consisting of 0.9 molar fraction helium, where the rest of the gas stream is made up by the mixture under investigation. This means 0.02 molar fraction CO_2 and 0.08 molar fraction H_2 for the simplified gas stream. Similarly for the more complicated gas stream we simply divide the molar fractions of all components by 10. Lastly, the density of the framework has to be specified. For ITQ-12 this is 1792 kg/m^3. The results will be compared for varying column lengths and the impact of the gas feed velocity on the breakthrough curves will be examined as well. To gain additional insight into the dependency of retention times (see section 4.7 in the work of S. Sharma et al. [19]) on column length and gas feed velocity, the Origin software will be used to create fits.

3. Results

To validate the aforementioned methods, excess adsorption isotherms computed using these methods will be compared to experimental and simulated adsorption isotherms from literature. It should be noted that the models used in this work have already been validated in other works. In particular the adsorbate models have been validated for general zeolites.

The first step in the validation of the models used in this work is to verify that the forcefield and adsorbates are modeled accurately. This means the way the framework is modeled is not yet taken into account. To do this, the MFI zeolite is used instead of ITQ-12. This was chosen since MFI is also a pure silica zeolite which means that no additional interactions have to be specified in the forcefield. Furthermore both experimental and simulated adsorption isotherms of hydrogen and carbon dioxide (the main components of the SMR product stream) are readily available for this zeolite. The forcefield and adsorbate models are used to compute adsorption isotherms for hydrogen at 90 K and carbon dioxide at 303 K. The result is included in Fig. 1. For both situations the obtained data has been compared to both existing experimental data as well as data from previous simulations. As can be observed the values resulting from simulations are in agreement with published data.

To validate the simulation of the ITQ-12 zeolite framework, the simulation has to be compared to existing data concerning ITQ-12. Luckily, experimentally obtained adsorption isotherm data is available for both carbon dioxide and methane in ITQ-12 [17]. Three possible ways to model the ITQ-12 framework have been considered for this work. These are referred to as ITQ-12, ITQ-12bis and ITW. ITQ-12 and ITQ-12bis correspond to real life synthesized instances of the zeolite and their reported topologies. ITW is the theoretical shape of the zeolite. One of the questions to be answered is which framework model best reproduces the experimental data found by E. Pérez-Botella et al. [17]. To do this, adsorption isotherms of CO_2 and CH_4 at 303 K were computed for all three framework models. For these computations, it was necessary to first compute the helium void fraction for all three frameworks (Table 2). The resulting adsorption isotherms are included in Fig. 2(a) for CO_2 and Fig. 3 for CH_4. For CO_2, quite a large discrepancy was found between the data from simulations in this work and experimental data. A possible explanation for this is that E. Pérez-Botella et al. [17] report a rather high value for the available pore volume compared to values obtained in this work through simulations in RASPA (see Table 2). Applying correction factors based on the available pore volumes results in Fig. 2(b). It is clear that the agreement is already somewhat better, though still not ideal. For methane the agreement with experimental data is much better for all three models. Clearly ITQ-12 and ITW show the better agreement for low pressures while for higher pressures the ITQ-12bis model performs best. In the end the decision was made to use the ITQ-12 framework model for further simulations since the ITQ-12 structure can be produced in real life and is therefore more relevant for the industry compared to ITW. Additionally the CO_2 adsorption results for ITQ-12 using the correction factor are not much worse than the ITW results, especially at lower pressures. On top of this, there is only one set of experimental data available for CO_2 adsorption which means that there is a possibility of erroneous experimental data. Ideally the validation would use multiple sets of independently obtained experimental data. The decision to use the ITQ-12 model was based mostly on the CO_2 adsorption results since this is a more important component than CH_4.

Having successfully validated the model, the first items of interest are the mixture adsorption isotherms of the hydrogen/carbon dioxide mixture as well as the full mixture as shown in Table 1. All isotherms are computed at 311 K corresponding to the gas stream leaving the low-temperature shift in the work of J. C. Molburg and R. D. Doctor [6]. Although the isotherms are computed for a range of pressures, it is ensured that the experimental pressure of 1.6 $\cdot 10^3$ kPa reported in the work of J. C. Molburg and R. D. Doctor [6] is also included. Where

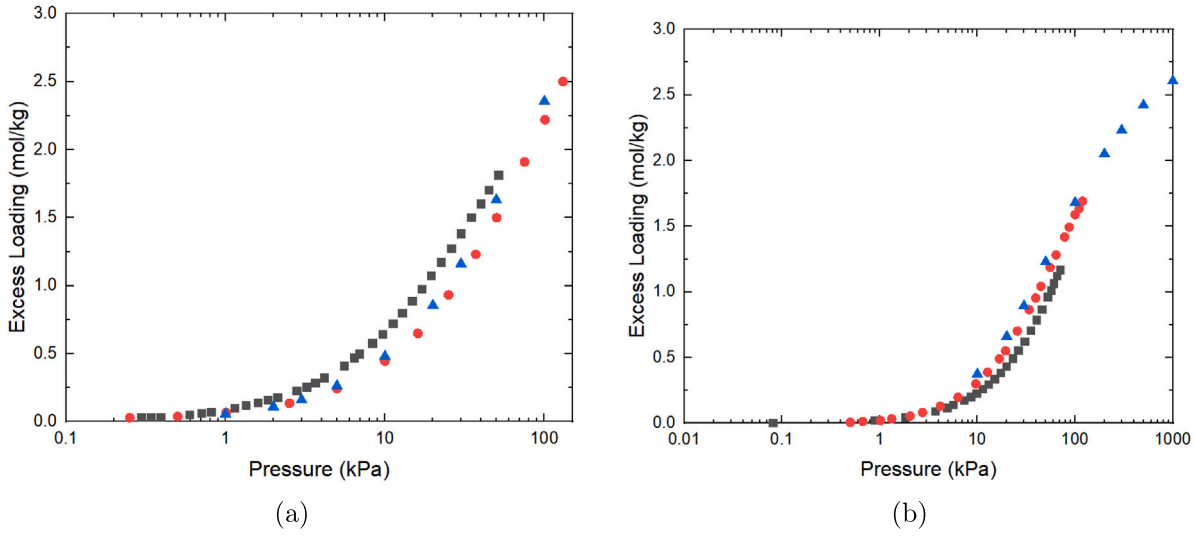

Fig. 1. Validation of forcefield and adsorbate modeling using existing data for MFI zeolite. Blue triangles: own data. Red circles: Existing data from simulation. Gray squares: Existing experimental data. (a) Excess adsorption isotherms for hydrogen in the MFI zeolite at 90 K. Experimental and simulation data taken from the work of K. S. Deeg et al. [9] (Fig. 3). (b) Excess adsorption isotherms for carbon dioxide in the MFI zeolite at 303 K. Experimental and simulation data taken from the work of A. García-Sánchez et al. [30] (Fig. 5a). Uncertainties were verified to be smaller than datapoint markers for both graphs.

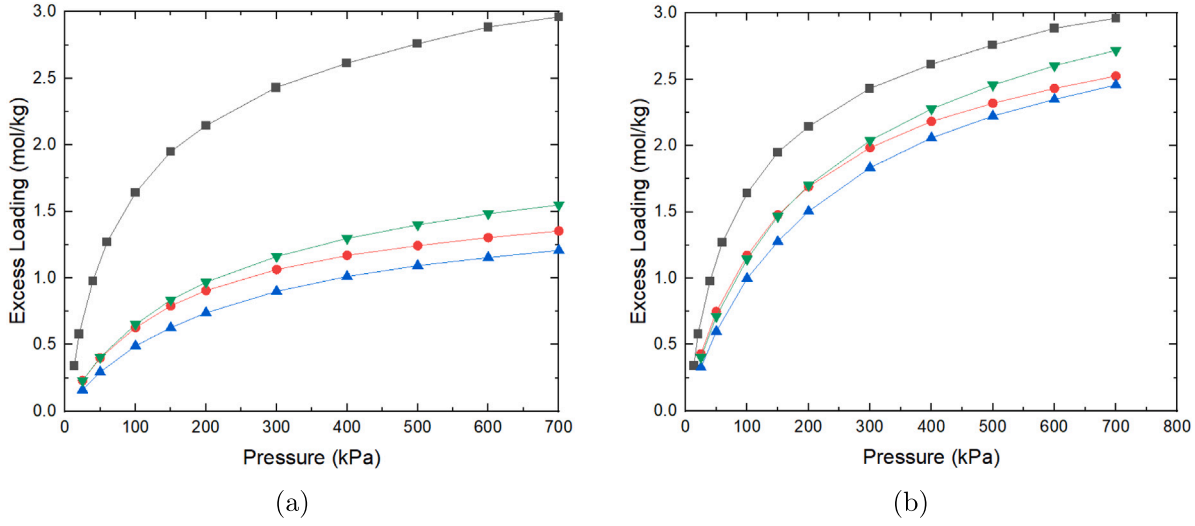

Fig. 2. Validation of carbon dioxide adsorption in zeolite and comparison of different framework models. Excess adsorption isotherms for carbon dioxide at 303 K. Gray squares: Experimental data taken from the work of E. Pérez-Botella et al. [17] (Fig. 4). Green reversed triangles: own data for ITW. Red circles: own data for ITQ-12. Blue triangles: own data for ITQ-12bis. (a) Simulation data for framework models ITQ-12, ITQ-12bis and ITW. (b) Simulation data for framework models ITQ-12, ITQ-12bis and ITW corrected based on available pore volume reported by E. Pérez-Botella et al. [17]. Uncertainties were verified to be smaller than datapoint markers for both figures.

relevant this pressure will be indicated in figures using a vertical dashed red line. Pure component absolute adsorption isotherms are computed for all components and then fitted using RUPTURA and the resulting parameters are used to compute mixture isotherms in RUPTURA using IAST. Both mixture isotherms are compared to the mixture isotherms obtained through RASPA to validate the use of IAST for breakthrough computations. After this, breakthrough curves are computed for both mixtures to investigate the feasibility of separating hydrogen from carbon dioxide/the full mixture in a pressure swing adsorption process.

An investigation of the pure component adsorption isotherms for hydrogen and carbon dioxide reveals that hydrogen adsorption is much lower than carbon dioxide adsorption at relevant pressures. A detailed discussion of these pure component adsorption isotherms can be found in Figure S4 of the ESI. Their best fits are included in Figure S5. Further fitting details can be found in Figure S6 and S7. Pure component adsorption isotherms of the other components as well as their best fits can be found in Figure S8, S9 and S10.

The next step is to consider the mixture adsorption isotherms that can be computed for the simple mixture consisting of 0.2 molar fraction CO_2 and 0.8 molar fraction H_2. Such isotherms were computed using RASPA and RUPTURA and are included in Fig. 4. Since these are mixture adsorption isotherms, they concern the competitive adsorption of CO_2 and H_2. Competitive adsorption in zeolites has been widely reported over the years. For adsorption molecules without a dipole, like carbon dioxide and hydrogen, the competitive adsorption is similar to that of non-polar hydrocarbons [43]. At low values of pressure, the bigger molecule always adsorbs over the smaller molecule for enthalpic effect, i.e. the heat of adsorption of carbon dioxide is much higher than that of hydrogen. At intermediate values of pressure, the commonly called length enthalpy effect favors the larger carbon dioxide over the shorter hydrogen. This effect can be seen in Fig. 4, where, despite being in much lower proportion, for increasing values of pressure, carbon dioxide adsorption dominates until the remaining space inside the zeolite is not enough for more molecules of this gas to be adsorbed,

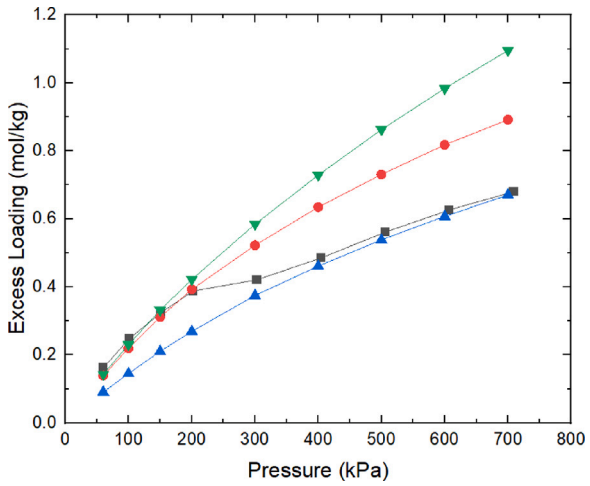

Fig. 3. Validation of methane adsorption in zeolite and comparison of different framework models. Excess adsorption isotherms for methane at 303 K. Gray squares: Experimental data taken from the work of E. Pérez-Botella et al. [17] (Fig. 4). Green reversed triangles: own data for ITW. Red circles: own data for ITQ-12. Blue triangles: own data for ITQ-12bis. Uncertainties were verified to be smaller than datapoint markers.

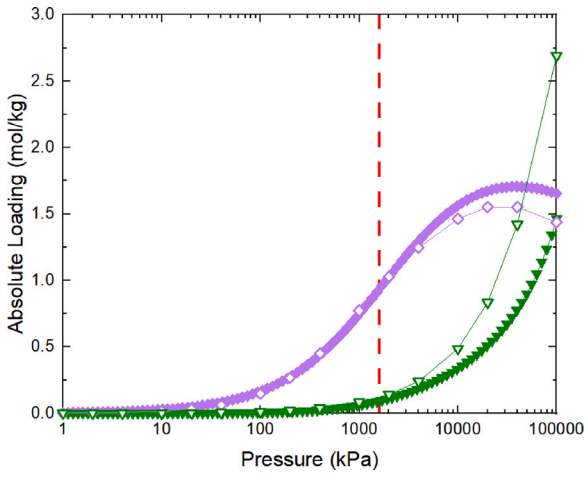

Fig. 4. Comparison of mixture adsorption isotherms of hydrogen and carbon dioxide in ITQ-12 at 311 K using RASPA and RUPTURA for a mixture containing 0.8 molar fraction hydrogen and 0.2 molar fraction carbon dioxide. Green reversed triangles: hydrogen. Purple diamonds: carbon dioxide. Empty symbols: result of simulations using RASPA. Filled symbols: result of simulations using RUPTURA. Uncertainties were verified to be smaller than datapoint markers. Experimental pressure of $1.6 \cdot 10^3$ kPa indicated with dashed red line.

after which the adsorption of hydrogen is favored. This is commonly called the size entropy effect. Based on the RASPA mixture adsorption isotherm, selectivity plots can be created for both components. Such selectivity plots can be found in Figure S11 of the ESI. Comparing the mixture adsorption isotherm computed using RASPA to the predicted mixture adsorption isotherm using IAST in RUPTURA it can be seen that there is a nice agreement on the general shapes of the adsorption isotherms. However, the hydrogen adsorption according to RUPTURA is significantly lower than the hydrogen adsorption according to RASPA and the carbon dioxide adsorption according to RUPTURA is somewhat higher than the carbon dioxide adsorption according to RASPA. In other words, the two methods agree on the qualitative behavior of the mixture adsorption but not on the quantitative behavior. This disagreement is likely caused by the fact that IAST assumes that hydrogen acts as an ideal gas while in actuality it follows a somewhat different equation of state. In other words the mixture adsorption isotherm computed using RASPA is likely to be correct, while the prediction computed in RUPTURA is only an approximation. Since agreement between the two methods is rather close near the pressure that will be used in breakthrough curve computations ($1.6 \cdot 10^3$ kPa, dashed red line), it can be concluded that IAST can be used for breakthrough curve simulations.

The preferential adsorption of carbon dioxide over hydrogen observed in the previously computed adsorption isotherms translates into larger retention times in breakthrough calculations. Two example cases have been included in Fig. 5. Fig. 5(a) shows a breakthrough isotherm for high column length and low gas feed velocity. Fig. 5(b) shows a breakthrough isotherm for low column length and high gas feed velocity. Indeed, the results of breakthrough simulations for the simple mixture show that hydrogen travels through the column very fast due to its weak interactions with the zeolite, while carbon dioxide travels slower due to its stronger interaction with the zeolite. This means that for lower times there will be no CO_2 in the outgoing gas stream. Gradually, the amount of CO_2 exiting the column will increase until it is equal to the CO_2 concentration in the gas feed.

Increasing the column length indeed introduces longer retention times for CO_2, but seems to have little effect on the retention time of hydrogen. This means that longer columns will produce pure hydrogen just as fast as shorter ones and only lose purity at later times. Higher column length is therefore favorable as it results in better separation. The breakthrough curves of CO_2 are visualized for different column lengths in Fig. 6(a). See Figure S12a in the ESI for a more in depth discussion of the effect of changing the column length. Lowering the gas feed velocity has a similar effect as increasing the column length. Again the H_2 retention times stay roughly the same while the CO_2 retention times increase. The breakthrough curves of CO_2 are visualized for different gas feed velocities in Fig. 6(b). See Figure S12b in the ESI for a more in depth discussion of the effect of changing the gas feed velocity. Full breakthrough curves that were used to derive the above results are included in the supporting information (Figure S13 and S14). The question remains what the optimal column length and gas feed velocity to be used are. This ultimately depends on the amount of gas to be separated, but it is clear that the separation of hydrogen from carbon dioxide works best for relatively high column lengths and low gas feed velocities since the difference in retention time between H_2 and CO_2 is the largest under these conditions. It should be noted that under these conditions the rate at which purified hydrogen is produced is relatively low and the volume of the column is relatively high. Therefore it is clear that in industrial practice we cannot simply keep increasing the column length and gas feed velocity, as there is a tradeoff between the amount of separation and the rate of hydrogen production per unit of column volume. After a batch of gas has been purified, the CO_2 that is trapped in the zeolite still needs to be removed. For this process the column length cannot be adjusted, but the gas feed velocity can. Therefore it is recommended to use long columns and low gas feed velocities for the separation process, while using higher gas feed velocities for the removal of CO_2 from the structure.

The next step is to analyze the mixture in full detail. This will allow a more realistic insight into the performance of the ITQ-12 zeolite when separating H_2 from the other mixture components. Besides making the results more realistic, this step also adds complexity to the study and allows for an analysis of the interference of the other components with hydrogen in the adsorption process. In Fig. 7, the full mixture adsorption isotherms are included for both RASPA and RUPTURA. Again it can be observed that the agreement between the two methods is rather close, especially around the industrially relevant pressure of $1.6 \cdot 10^3$ kPa. Therefore the usage of IAST in RUPTURA to predict mixture adsorption has been successfully validated and this method can be used in the prediction of breakthrough curves for the full mixture. It should be noted that the low adsorption of N_2 and CO is largely due to their low concentrations in the mixture. The supporting information contains a slightly more detailed investigation of the full mixture isotherm (Figure S15).

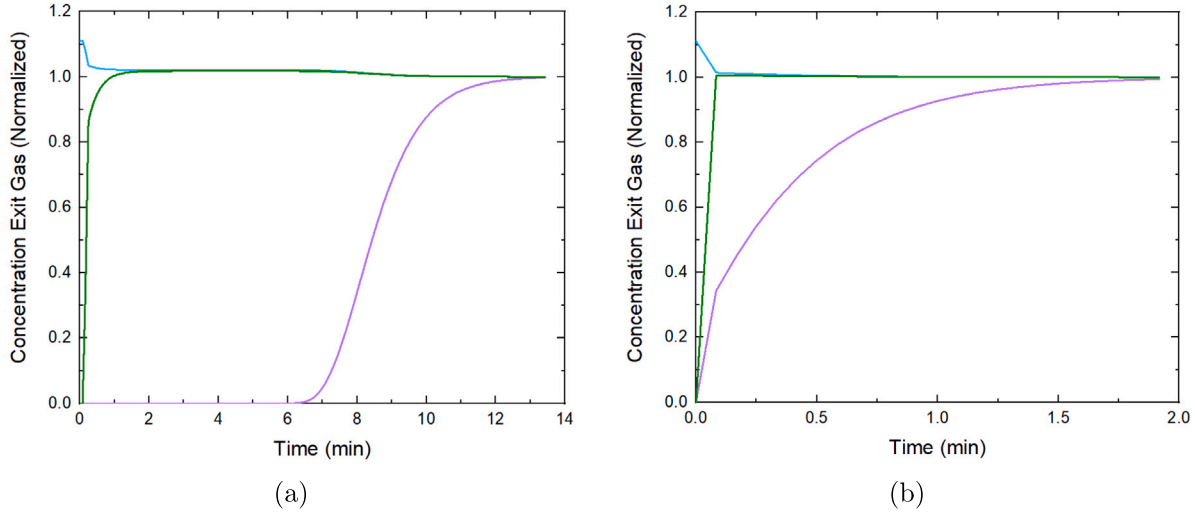

Fig. 5. Breakthrough curves for 0.02 molar fraction CO_2 (purple), 0.08 molar fraction H_2 (green) and 0.9 molar fraction He (light blue) in ITQ-12 at 311 K and $16{\cdot}10^5$ Pa. (a) Breakthrough curve with a column length of 0.5 m and gas feed velocity of 0.05 m/s (i.e. the slowest conditions that were investigated). (b) Breakthrough curve with a column length of 0.1 m and gas feed velocity of 0.25 m/s (i.e. the fastest conditions that were investigated).

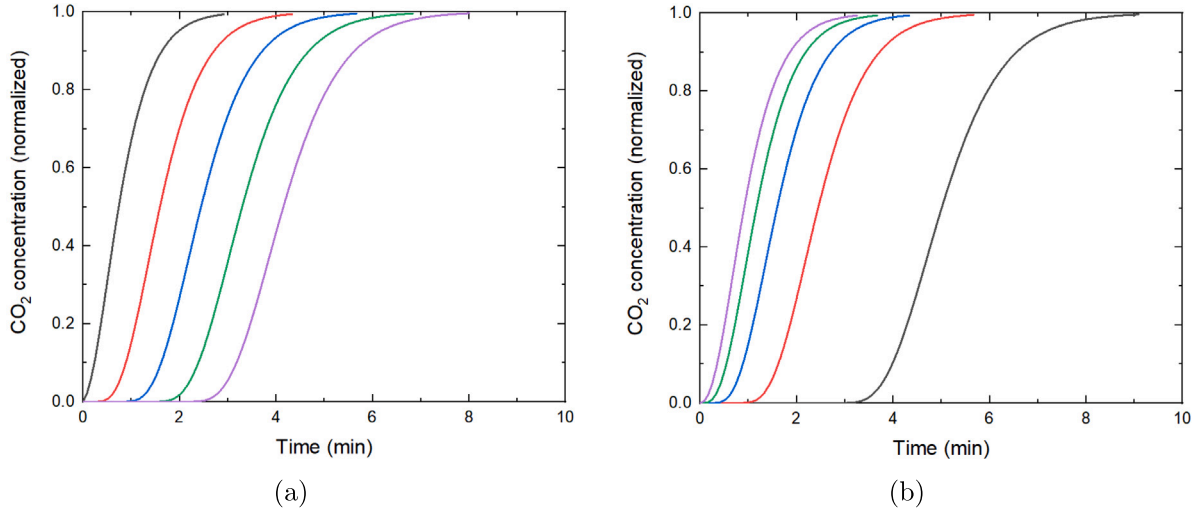

Fig. 6. CO_2 breakthrough curves for 0.02 molar fraction CO_2, 0.08 molar fraction H_2 and 0.9 molar fraction He mixture in ITQ-12 at 311 K and $16{\cdot}10^5$ Pa. Visualizing the dependency on column length and gas feed velocity. (a) Breakthrough curves for several column lengths. Column length of: Gray: 0.1 m, Red: 0.2 m, Blue: 0.3 m, Green: 0.4 m, Purple: 0.5 m. Gas feed velocity 0.1 m/s. (b) Breakthrough curves for several gas feed velocities. Gas feed velocity: Gray: 0.05 m/s, Red: 0.10 m/s, Blue: 0.15 m/s, Green: 0.20 m/s, Purple: 0.25 m/s. Column length 0.3 m.

Examining the breakthrough curves for the full mixture, such as the example breakthrough curve in Fig. 8, it can be seen that Hydrogen is still the component that travels through the ITQ-12 zeolite the fastest. It is also clear that the conditions used in this example breakthrough curve would not allow for a good separation between hydrogen and the other stream components, as the retention times of CO and N_2 are nearly equal to 0 (just like the retention time of H_2). The retention time for CH_4 seems to be around one third of a minute while CO_2 starts to exit the column slightly before the one minute mark. From this it is also clear that the separation between H_2 and CO_2 remains rather large even when the other components are added. Indeed, the influence of carbon monoxide and nitrogen on this separation is almost negligible due to their low presence in the mixture. The effect of methane is slightly larger, but still low enough so as to not interfere with the separation of hydrogen from carbon dioxide. Additionally methane also shows an acceptable separation from hydrogen in breakthrough analysis. The only difficulty therefore might be to distinguish between hydrogen, nitrogen and carbon monoxide during breakthrough analysis as their low adsorption is translated into very short retention times. This could possibly be addressed by optimizing the breakthrough parameter of column length and gas feed velocity (as can be seen for example in Figures S16, S19 and S20 in the supporting information). Alternatively, the use of ITQ-12 could be combined with other separation techniques. In current industrial PSA processes for the purification of the SMR product stream, activated carbons (ACs) are often used together with zeolites [44]. In such processes ACs are used for the removal of CO_2 and CH_4 [45,46], while zeolites, such as 5A, take off CO and N_2. Our findings suggest that the ITQ-12 zeolite could replace these activated carbons while the other unwanted components could be removed through other methods. It is also possible to investigate the dependency of the breakthrough curves for the full mixture on the column length and gas feed velocity, as has been done in Fig. 6 for CO_2 in the simple mixture. The supporting information for this work contains such an analysis for all different components of the full mixture (Figures S16 through S20). It is additionally possible to compare the behavior of CO_2 and H_2 for the breakthrough curves computed for the simple and full mixtures. This is done in Figure S21 in the ESI. The difference is found to be negligible. Therefore it can be concluded that adding the other

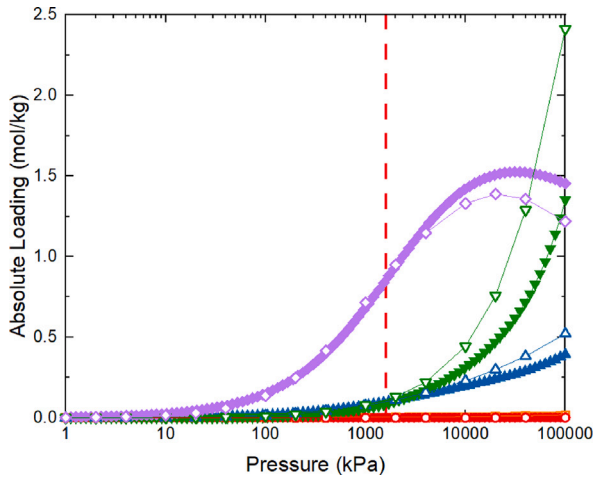

Fig. 7. Comparison of mixture adsorption isotherms of full mixture (excluding water) in ITQ-12 at 311 K using RASPA and RUPTURA. Green reversed triangles: hydrogen. Purple diamonds: carbon dioxide. Orange squares: nitrogen. Red circles: carbon monoxide. Blue triangles: methane. Empty symbols: result of simulations using RASPA. Filled symbols: result of simulations using RUPTURA. Uncertainties were verified to be smaller than datapoint markers. Experimental pressure of $1.6 \cdot 10^3$ kPa indicated with dashed red line. Mixture components and their molar fractions: hydrogen — 0.74106, carbon dioxide — 0.18505, methane — 0.06882, nitrogen — 0.00401 and carbon monoxide — $1.03615 \cdot 10^{-4}$.

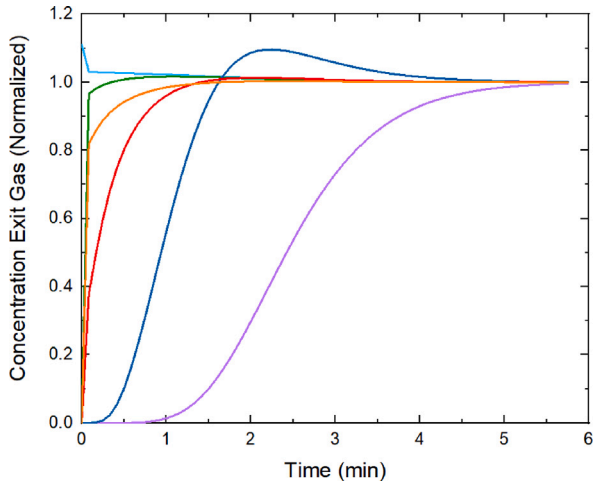

Fig. 8. Breakthrough curve of full mixture. Column length equal to 0.3 m, gas feed velocity equal to 0.1 m/s. Light blue: helium. Purple: carbon dioxide. Green: hydrogen. Dark blue: methane. Red: carbon monoxide. Orange: nitrogen. Mixture components and their molar fractions: hydrogen — 0.074106, carbon dioxide — 0.018505, methane — 0.006882, nitrogen — 0.000401, carbon monoxide — $1.03615 \cdot 10^{-5}$ and helium — 0.9.

mixture components does not significantly influence the behavior of CO_2 and H_2 as they move through the zeolite.

4. Conclusion

This work is an investigation of the suitability of the ITQ-12 zeolite for the separation of hydrogen from an SMR product stream. Investigation of the mixture adsorption isotherms at 'real' conditions found in industrial practice (i.e. conditions typical for an SMR product stream), revealed a rather high selectivity for CO_2 over H_2 in the ITQ-12 zeolite. In particular, the CO_2 selectivity is rather high around industrially relevant pressures. Based on the breakthrough curves examined in this work it seems quite feasible to use a column adsorption experiment for the separation of hydrogen from carbon dioxide. Indeed there is a large difference in retention times, as hydrogen exits the column rather quickly, while the retention time of carbon dioxide is relatively high and also shows greater dependency on the column length. The separation of hydrogen from the other components in the full mixture is less ideal as the difference in retention times is considerably smaller, especially for CO and N_2. To combat this, longer column lengths could be used. Alternatively, ITQ-12 could be used to remove mainly CO_2 and CH_4 from the mixture, while the other components are removed through other methods.

As the scope of this work is rather limited there still remains a plethora of unanswered questions and options for further research. First of all a sizeable discrepancy was uncovered between experimental data and the simulations using RASPA. A possible explanation has already been posed as there is a rather large difference in the reported available pore volume. However, the reason for this large difference is still unknown. Second of all, while the experimental conditions for the temperature and pressure have been taken from literature, there is a rather large variance in these values between different descriptions of the SMR process. Therefore a more in-depth exploration of the experimental conditions in industrial practice could be beneficial. Lastly, the optimal values for the column length and gas feed velocity still have to be determined (perhaps with a set of specific applications in mind) and a more thorough research into the effect of these parameters on performance of a theoretical column adsorption experiment is still required. This work serves as a feasibility study of the use of the ITQ-12 zeolite. As such, a first indication of the potential use has been given. Indeed the results in this work are rather promising, as it seems that the zeolite could be useful for the separation of hydrogen from the other components in the SMR product stream.

CRediT authorship contribution statement

Jeroen van Heijst: Writing – original draft, Validation, Investigation, Data curation, Visualization, Formal analysis. **Ana Martin-Calvo:** Writing – review & editing, Funding adquisition, Project administration, Supervision, Resources, Formal analysis, Conceptualization. **Sofia Calero:** Writing – review & editing, Supervision, Resources, Project administration, Funding acquisition.

Declaration of competing interest

The authors declare no competing financial interests or personal relationships that could have appeared to influence the work reported in this work.

Data availability

Data will be made available on request.

Acknowledgments

A. Martin-Calvo thanks the Spanish Ministerio de Ciencia, Innovacion y Universidades (IJC2019-042207-I). We are gratefull to C3UPO for the HPC support.

Appendix A. Supplementary data

Supplementary material related to this article can be found online at https://doi.org/10.1016/j.seppur.2024.127895. Supporting information contains: Visualizations of the unit cell and channels of the ITQ-12 structure (Figure S1 and S2). A comparison of the pore size distributions of the ITQ-12, ITQ-12bis and ITW structures (Figure S3). Pure components adsorption isotherms for hydrogen and carbon dioxide (Figure S4) as well as their best fits (Figure S5). Additional visualizations of the different fitting methods tried for hydrogen and carbon dioxide, as well as the values resulting from the best fit (Figure S6 and S7). Pure component adsorption isotherms for the components

that are unique to the full mixture, as well as visualizations of their best fits and resulting fitting values (Figure S8, S9 and S10). Selectivity plots based on the adsorption isotherm computed for the hydrogen/carbon dioxide mixture (Figure S11). An investigation of the effect of changing the column length and gas feed velocity in a breakthrough experiment for the hydrogen/carbon dioxide mixture (Figure S12). Breakthrough curves for the hydrogen/carbon dioxide mixture for varying gas feed velocities and column lengths (Figure S13 and S14). A visualization of the full mixture adsorption isotherm where N_2 and CO are visualized separately for better visual inspection (Figure S15). Analysis of the dependency of H_2, CO_2, CH_4, N_2 and CO breakthrough curves on column length and gas feed velocity (Figures S16 through S20). Comparison of breakthrough curves of hydrogen and carbon dioxide in the simplified mixture with breakthrough curves of the same components in the full mixture (Figure S21).

References

[1] Seyed Ehsan Hosseini, Mazlan Abdul Wahid, Hydrogen from solar energy, a clean energy carrier from a sustainable source of energy, Int. J. Energy Res. 44 (2020) 4110–4131.

[2] Hydrogen production and storage: R & D priorities and gaps, 2006.

[3] A. Boyano, A.M. Blanco-Marigorta, T. Morosuk, G. Tsatsaronis, Exergoenvironmental analysis of a steam methane reforming process for hydrogen production, Energy 36 (2011) 2202–2214.

[4] Xiucheng Huang, Ana Martín-Calvo, Martijn J.J. Mulder, Sjoerd C.J. van Acht, Juan José Gutiérrez-Sevillano, Julio C. García-Navarro, Sofía Calero, Effect of zeolitic imidazolate framework topology on the purification of hydrogen from coke oven gas, ACS Sustain. Chem. Eng. 11 (2022) 8020–8034.

[5] Noureddine Hajjaji, Marie Noëlle Pons, Ammar Houas, Viviane Renaudin, Exergy analysis: An efficient tool for understanding and improving hydrogen production via the steam methane reforming process, Energy Policy 42 (2012) 392–399.

[6] John Molburg, Richard D. Doctor, Hydrogen from steam-methane reforming with CO2 capture, in: International Pittsburgh Coal Conference Proceedings: Twentieth Annual International Pittsburgh Coal Conference September 15-19 2003 Pittsburgh Pennsylvania USA. Pittsburgh Coal Conference, 2003.

[7] Hind Jihad Kadhim Shabbani, Ili Khairunnisa Shamsudin, Nurhafiza Natasha Dezaini, Ammar Ali Abd, Mohd Roslee Othman, Effect of adsorption–desorption on hydrogen purity and recovery in non-adiabatic pressure swing mediated by microporous palm kernel shell adsorbent, Fuel 311 (2022) 122550.

[8] Kingsley Christian Kemp, Jung Gi Min, Hyun June Choi, Suk Bong Hong, Small gas adsorption and separation in small-pore zeolites, in: Susana Valencia, Fernando Rey (Eds.), New Developments in Adsorption/Separation of Small Molecules By Zeolites, Springer International Publishing, Cham, 2020, pp. 1–30.

[9] Kathryn S. Deeg, Juan José Gutiérrez-Sevillano, Rocío Bueno-Pérez, José B. Parra, Conchi O. Ania, Manuel Doblaré, Sofía Calero, Insights on the molecular mechanisms of hydrogen adsorption in zeolites, J. Phys. Chem. C 117 (2013) 14374–14380.

[10] Jorge A. Brizuela-Mendoza, Felipe D.J. Sorcia-Vázquez, Jesse Y. Rumbo-Morales, Gerardo Ortiz-Torres, Carlos Alberto Torres-Cantero, Mario A. Juárez, Omar Zatarain, Moises Ramos-Martinez, Estela Sarmiento-Bustos, Julio C. Rodríguez-Cerda, Juan Carlos Mixteco-Sánchez, Hector Miguel Buenabad-Arias, Pressure swing adsorption plant for the recovery and production of biohydrogen: Optimization and control, Processes 11 (2023) 2997.

[11] Jesse Y. Rumbo-Morales, Gerardo Ortiz-Torres, Estela Sarmiento-Bustos, Antonio Márquez Rosales, Manuela Calixto-Rodriguez, Felipe D.J. Sorcia-Vázquez, Alan F. Pérez-Vidal, Julio C. Rodríguez-Cerda, Purification and production of bio-ethanol through the control of a pressure swing adsorption plant, Energy 288 (2024).

[12] Jesse Y. Rumbo Morales, Guadalupe López López, Víctor M. Alvarado Martínez, Felipe de J. Sorcia Vázquez, Jorge A. Brizuela Mendoza, Mario Martínez García, Parametric study and control of a pressure swing adsorption process to separate the water-ethanol mixture under disturbances, Sep. Purif. Technol. 236 (2019) 116214.

[13] Jesse Y. Rumbo Morales, Gerardo Ortiz-Torres, Rodolfo Omar Domínguez García, Carlos Alberto Torres Cantero, Manuela Calixto Rodriguez, Estela Sarmiento-Bustos, Edén Oceguera-Contreras, Alberto Arturo Flores Hernández, Julio César Rodríguez Cerda, Yehoshua Aguilar Molina, Mario Martínez García, Review of the pressure swing adsorption process for the production of biofuels and medical oxygen: Separation and purification technology, Adsorpt. Sci. Technol. 2022 (2022).

[14] Philip A. Barrett, Teresa Boix, Marta Puche, David H. Olson, Edgar Jordan, Hubert Koller, Miguel A. Camblor, ITQ-12: A new microporous silica polymorph potentially useful for light hydrocarbon separations, Chem. Commun. 3 (2003) 2114–2115.

[15] David H. Olson, Xiaobo Yang, Miguel A. Camblor, ITQ-12: A zeolite having temperature dependent adsorption selectivity and potential for propene separation, J. Phys. Chem. B 108 (2004) 11044–11048.

[16] Xiaobo Yang, Miguel A. Camblor, Yongjae Lee, Haiming Liu, David H. Olson, Synthesis and crystal structure of as-synthesized and calcined pure silica zeolite ITQ-12, J. Am. Chem. Soc. 126 (2004) 10403–10409.

[17] Eduardo Pérez-Botella, Miguel Palomino, Gabriel B. Báfero, Heloise O. Pastore, Susana Valencia, Fernando Rey, The influence of zeolite pore topology on the separation of carbon dioxide from methane, J. CO2 Util. 72 (2023) 102490.

[18] David Dubbeldam, Sofía Calero, Donald E. Ellis, Randall Q. Snurr, RASPA: Molecular simulation software for adsorption and diffusion in flexible nanoporous materials, Mol. Simul. 42 (2015) 81–101.

[19] Shrinjay Sharma, Salvador R.G. Balestra, Richard Baur, Umang Agarwal, Erik Zuidema, Marcello S. Rigutto, Sofia Calero, Thijs J.H. Vlugt, David Dubbeldam, RUPTURA: simulation code for breakthrough, ideal adsorption solution theory computations, and fitting of isotherm models, Mol. Simul. 49 (2023) 893–953.

[20] David Dubbeldam, Ariana Torres-Knoop, Krista S. Walton, On the inner workings of Monte Carlo codes, Mol. Simul. 39 (2013) 1253–1292.

[21] Tina Düren, Lev Sarkisov, Omar M. Yaghi, Randall Q. Snurr, Design of new materials for methane storage, Langmuir 20 (2004) 2683–2689.

[22] Juan José Gutiérrez-Sevillano, Sofía Calero, Computational approaches to zeolite-based adsorption processes, in: Susana Valencia, Fernando Rey (Eds.), New Developments in Adsorption/Separation of Small Molecules By Zeolites, Springer International Publishing, Cham, 2020, pp. 57–83.

[23] Ch. Baerlocher, Darren Brouwer, Bernd Marler, L.B. McCusker, Database of Zeolite Structures, https://www.iza-structure.org/databases.

[24] Orhan Talu, Allan L. Myers, Molecular simulation of adsorption: Gibbs dividing surface and comparison with experiment, AIChE J. 47 (2004) 1160–1168.

[25] Tina Düren, Franck Millange, Gérard Férey, Krista S. Walton, Randall Q. Snurr, Calculating geometric surface areas as a characterization tool for metal - Organic frameworks, J. Phys. Chem. C 111 (2007) 15350–15356.

[26] Lev Sarkisov, Alex Harrison, Computational structure characterisation tools in application to ordered and disordered porous materials, Mol. Simul. 37 (2011) 1248–1257.

[27] Lev D. Gelb, K.E. Gubbins, Pore size distributions in porous glasses: A computer simulation study, Langmuir 15 (1999) 305–308.

[28] Ana Martín-Calvo, Elena García-Pérez, Almudena García-Sánchez, Rocío Bueno-Pérez, Said Hamad, Sofia Calero, Effect of air humidity on the removal of carbon tetrachloride from air using Cu–BTC metal–organic framework, Phys. Chem. Chem. Phys. 13 (2011) 11165–11174.

[29] Ana Martín-Calvo, Francisco D. Lahoz-Martín, Sofía Calero, Understanding carbon monoxide capture using metal–organic frameworks, J. Phys. Chem. C 116 (2012) 6655–6663.

[30] Almudena García-Sánchez, Conchi O. Ania, José B. Parra, David Dubbeldam, Thijs J.H. Vlugt, Rajamani Krishna, Sofía Calero, Transferable force field for carbon dioxide adsorption in zeolites, J. Phys. Chem. C 113 (2009) 8814–8820.

[31] D. Dubbeldam, S. Calero, T.J.H. Vlugt, R. Krishna, T.L.M. Maesen, B. Smit, United atom force field for alkanes in nanoporous materials, J. Phys. Chem. B 108 (2004) 12301–12313.

[32] David Dubbeldam, Krista S. Walton, Thijs J.H. Vlugt, Sofia Calero, Design, parameterization, and implementation of atomic force fields for adsorption in nanoporous materials, Adv. Theory Simul. 2 (2019) 1900135 (1/62)–1900135 (62/62).

[33] M.P. Allen, D.J. Tildesley, Computer Simulation of Liquids, Clarendon Press, Oxford, 1991.

[34] T. J.H. Vlugt, E. García-Pérez, D. Dubbeldam, S. Ban, S. Calero, Computing the heat of adsorption using molecular simulations: The effect of strong Coulombic interactions, J. Chem. Theory Comput. 4 (2008) 1107–1118.

[35] H. van Koningsveld, H. van Bekkum, J.C. Jansen, On the location and disorder of the tetrapropylammonium (TPA) ion in zeolite ZSM-5 with improved framework accuracy, Acta Crystallogr. Sect. B Struct. Sci. 43 (1987) 127–132.

[36] Robert Sips, On the structure of a catalyst surface, J. Chem. Phys. 16 (1948) 490–495.

[37] J. Tóth, State equation of the solid-gas interface layers, Acta Chimica Hung. 69 (1971) 311–328.

[38] József Tóth, Uniform interpretation of gas/solid adsorption, Adv. Colloid Interface Sci. 55 (1995) 1–239.

[39] Tóth J., Adsorption: Theory, Modeling and Analysis, Marcel Dekker Inc, New York, 2002.

[40] C. Boedeker, Über das verhältnis zwischen masse und wirkung beim kontakt ammoniakalscher flüssigkeiten mit ackererde und mit kohlensaurem kalk, ZA Pflanzenbau 7 (1859) 48–58.

[41] Irving Langmuir, The adsorption of gases on plane surfaces of glass, Mica and platinum, J. Am. Chem. Soc. 40 (1918) 1361–1403.

[42] Robert A. Koble, Thomas E. Corrigan, Adsorption isotherms for pure hydrocarbons, Ind. Eng. Chem. 44 (1952) 383–387.

[43] Rajamani Krishna, Berend Smit, Sofia Calero, Entropy effects during sorption of alkanes in zeolites, Chem. Soc. Rev. 31 (2002) 185–194.

[44] Filipe V.S. Lopes, Carlos A. Grande, Ana M. Ribeiro, José M. Loureiro, Oikonomopoulos Evaggelos, Vladimiros Nikolakis, Alírio E. Rodrigues, Adsorption of H_2, CO_2, CH_4, CO, N_2 and H_2O in activated carbon and zeolite for hydrogen production, Sep. Sci. Technol. 44 (2009) 1045–1073.

[45] Carlos A. Grande, Filipe V.S. Lopes, Ana M. Ribeiro, José M. Loureiro, Alírio E. Rodrigues, Adsorption of off-gases from steam methane reforming (H_2, CO_2, CH_4, CO and N_2) on activated carbon, Sep. Sci. Technol. 43 (2008) 1338–1364.

[46] Mario Martínez García, Jesse Y. Rumbo Morales, Gerardo Ortiz Torres, Salvador A. Rodríguez Paredes, Sebastián Vázquez Reyes, Felipe de J. Sorcia Vázquez, Alan F. Pérez Vidal, Jorge S. Valdez Martínez, Ricardo Pérez Zúñiga, Erasmo M. Renteria Vargas, Simulation and state feedback control of a pressure swing adsorption process to produce hydrogen, Mathematics 10 (2022) 1762.